



# CHORUS

This is the accepted manuscript made available via CHORUS. The article has been published as:

## Light-front holographic distribution amplitudes of pseudoscalar mesons and their application to B-meson decays

Qin Chang, Stanley J. Brodsky, and Xin-Qiang Li

Phys. Rev. D **95**, 094025 — Published 30 May 2017

DOI: [10.1103/PhysRevD.95.094025](https://doi.org/10.1103/PhysRevD.95.094025)

# Light-front holographic distribution amplitudes of pseudoscalar mesons and their application to $B$ -meson decays

Qin Chang<sup>a,b</sup>, Stanley J. Brodsky<sup>b</sup> and Xin-Qiang Li<sup>c</sup>

<sup>a</sup>Institute of Particle and Nuclear Physics, Henan Normal University, Henan 453007, China

<sup>b</sup>SLAC National Accelerator Laboratory, Stanford University, Stanford, CA 94309, USA

<sup>c</sup>Institute of Particle Physics and Key Laboratory of Quark and Lepton Physics (MOE),

Central China Normal University, Wuhan, Hubei 430079, China

## Abstract

In this paper the dynamical spin effects of the light-front holographic wavefunctions for light pseudoscalar mesons are studied. These improved wavefunctions are then confronted with a number of hadronic observables: the decay constants of  $\pi$  and  $K$  mesons, their  $\xi$ -moments, the pion-to-photon transition form factor, and the pure annihilation  $\bar{B}_s \rightarrow \pi^+\pi^-$  and  $\bar{B}_d \rightarrow K^+K^-$  decays. Taking  $f_\pi$ ,  $f_K$  and their ratio  $f_K/f_\pi$  as constraints, we perform a  $\chi^2$  analysis for the holographic parameters, including the mass scale parameter  $\sqrt{\lambda}$  and the effective quark masses, and find that the fitted results are in good consistence with the ones obtained from the light-quark hadronic Regge trajectories. In addition, we also show that the end-point divergence appeared in the pure annihilation  $\bar{B}_s \rightarrow \pi^+\pi^-$  and  $\bar{B}_d \rightarrow K^+K^-$  decays can be well controlled by using these improved light-front holographic distribution amplitudes.

# 1 Introduction

Light-front (LF) quantization is the natural frame-independent framework for the description of non-perturbative relativistic bound-state structure in quantum field theory. In principle, one can solve QCD by diagonalizing the LF QCD Hamiltonian  $H_{LF}$ , by using, for example, the discretized light-cone quantization method [1]. Both the spectrum and the LF wavefunctions (LFWFs), which encode all the hadronic information, are then obtained from the eigenvalues and eigenfunctions of the Heisenberg equation  $H_{LF}|\psi\rangle = M^2|\psi\rangle$ . The result is an infinite set of coupled integral equations for the LF components in a Fock expansion [1]. Unfortunately, solving these equations is a formidable computational task for the case of a non-abelian quantum field theory such as QCD in four-dimensional spacetime. Consequently, we have to resort to the alternative methods; recent comprehensive reviews of which could be found in Refs. [1, 2].

In recent years, a semiclassical first approximation to strongly coupled QCD — light-front holographic AdS/QCD — has been developed [3–7]. This approach to hadron dynamics in physical four-dimensional spacetime at fixed LF time  $\tau = x^+ = x^0 + x^3$  is holographically dual to the dynamics of a gravitational theory in five-dimensional anti-de Sitter (AdS) space. The LF eigenvalue equation can be reduced in this theoretical framework to an effective single-variable quantum-mechanical wave equation for  $\phi(\zeta)$  which is given by [7]

$$\left(-\frac{d^2}{d\zeta^2} - \frac{1 - 4L^2}{4\zeta^2} + U(\zeta)\right)\phi(\zeta) = M^2\phi(\zeta). \quad (1)$$

The function  $U(\zeta)$  is the effective potential acting on the valence states [8]; it is holographically related to a unique dilation profile in AdS space. As a result, one arrives at a concise form of a color-confining harmonic oscillator in impact space after the holographical mapping,  $U(\zeta, J) = \lambda^2\zeta^2 + 2\lambda(J - 1)$ . The emergence of the mass scale  $\lambda$  is consistent with the procedure of de Alfaro, Fubini, and Furlan [9] in which a mass scale can appear in a Hamiltonian without affecting the conformal invariance of the action [2]. With only one mass scale in addition to the quark masses, this color-confining approach predicts successfully the spectroscopy and some dynamical observables (like form factors and structure functions) of light-quark hadrons [3–6], as well as the behavior of the running coupling in the non-perturbative domain [10–12].

The eigenvalues of the light-front Schrödinger equation, Eq. (1), are the squares of the meson masses. The remarkably simple features of the empirical Regge trajectories for both

meson and baryon families are correctly reproduced by LF holographic QCD with only one parameter, the mass scale  $\lambda$  [13–17]. The eigensolutions of Eq. (1) provide the  $q\bar{q}$  light-front wavefunctions which control the dynamics of the mesons. After factoring out the longitudinal and orbital dependence, the LFWF can be written as

$$\psi(x, \zeta, \varphi) = e^{iL\varphi} X(x) \frac{\phi(\zeta)}{\sqrt{2\pi\zeta}}, \quad (2)$$

where  $\zeta^2 = x(1-x)\mathbf{b}_\perp^2$  is the Poincare' invariant radial variable of LF Hamiltonian, and  $\mathbf{b}_\perp$  is the invariant transverse impact variable. The hadronic LFWF  $\phi(\zeta)$  in the soft-wall holographic model encodes the dynamical properties of the mesons. If one also includes the light-quark masses, it is given by [5, 18]

$$\psi(x, \zeta) = \sqrt{\frac{\lambda}{\pi}} \sqrt{x(1-x)} e^{-\frac{\lambda\zeta^2}{2}} e^{-\frac{1}{2\lambda}(\frac{m_q^2}{x} + \frac{m_{\bar{q}}^2}{1-x})} \quad (3)$$

in impact space. Note that the LF kinetic energy  $\sum_i (\frac{k_i^2 + m^2}{x})_i$  is also the invariant mass squared  $\mathcal{M}^2 = (\sum_i k_i^\mu)^2$  of the hadronic constituents.

The holographic LFWF given by Eq. (3) has been successfully used to describe diffractive  $\rho$  meson electroproduction at HERA [19] as well as the spectroscopy and distribution amplitudes of light and heavy mesons [20–24]. After introducing the LF spinor structure of the wavefunctions for light vector mesons in analogy with that of the photon, the authors of Refs [25, 26] have predicted the light-front distribution amplitudes (LFDAs) of the  $\rho$  and  $K^*$  vector mesons, which were then used to evaluate the branching fractions of  $B \rightarrow \rho\gamma$  and  $B \rightarrow K^*\gamma$  decays. In addition, the  $B \rightarrow \rho, K^*$  form factors are computed and applied to rare  $B \rightarrow K^*\mu^+\mu^-$  and  $B \rightarrow \rho\ell\bar{\nu}_\ell$  decays [27–31]. Traditionally, the helicity dependence of the holographic LFWF is assumed to decouple from the dynamics, which leads to simple factorizable formulae for physical quantities, such as the decay constants [22, 23]. In Refs. [19, 25–31], the helicity dependence of the LFWFs for the vector mesons is introduced in order to predict specific helicity dependent observables.

In this paper, we will explore helicity-improved LFWFs for light pseudoscalar mesons, and then test their predictions for hadronic observables including the decay constants of  $\pi$  and  $K$  mesons, their  $\xi$ -moments and the pion-to-photon transition form factor. We will also explore their applications to two-body nonleptonic  $B$ -meson decays, focusing especially on the measured pure annihilation  $\bar{B}_s \rightarrow \pi^+\pi^-$  and  $\bar{B}_d \rightarrow K^+K^-$  decay channels.

In the past few years, several QCD-inspired approaches, such as QCD factorization (QCDF) [32–34], perturbative QCD (pQCD) [35, 36] and soft-collinear effective theory (SCET) [37–40], have been developed in order to evaluate the hadronic matrix elements of local operators which control two-body nonleptonic  $B$ -meson decays. However, the convolution integrals of the hard kernels with the asymptotic forms of distribution amplitudes of light final states suffer from an end-point divergence, such as  $\int_0^1 du/u$  or  $\int_0^1 du/(1-u)$ . This divergence limits the prediction power of the theoretical approaches and introduces large theoretical uncertainties.

Several schemes for regulating the end-point divergences have been previously proposed. In the SCET approach, a zero-bin subtraction [41] is assumed, and the annihilation diagrams are found to be factorizable and bring no any strong phase in the leading order of  $\mathcal{O}(\alpha_s(m_b)\Lambda_{\text{QCD}}/m_b)$  [42]. In the pQCD approach, the end-point singularity is avoided by introducing parton transverse momentum  $k_T$ , but at the expense of having to model the additional  $k_T$  dependence of the meson distributions; this predicts a large complex annihilation correction [35, 36, 43]. In the QCDF approach, the end-point divergent integrals are treated as signals of infrared-sensitive contributions which are parameterized by introducing a complex quantity  $X_A$  [44, 45]. Alternatively, one can also introduce an infrared-finite dynamical gluon propagator which moves the end-point singularity into an integral over the time-like gluon momentum; the divergence then vanishes, and a large strong phase is predicted [46, 47]. In contrast, in the LF holographic QCD, it can be seen from Eq. (3) that the end-point behavior is naturally suppressed by the exponential factor in LFWF due to non-vanishing effective quark masses,  $m_q$  and  $m_{\bar{q}}$ . Therefore, it is expected that the problem of end-point divergences can possibly be mitigated by the improved behavior of the LFWF near the end-points. In this paper we will test if the effective quark mass regulation of the end-point divergences can provide viable predictions for the pure annihilation heavy hadron decays.

Our paper is organized as follows. In section 2, the connections between holographic LFWFs and LFDAs for light pseudoscalar mesons are explored within the framework of LF quantization. Sections 3 and 4 are devoted to numerical results and discussions in which the decay constants, the  $\xi$ -moments and the pion-to-photon transition form factor are evaluated using the helicity-improved LFWFs and LFDAs. In section 5, the pure annihilation  $\bar{B}_s \rightarrow \pi^+\pi^-$  and  $\bar{B}_d \rightarrow K^+K^-$  decays are studied in detail using the LFDAs. Finally, we give our summary in section 6.

## 2 The holographic light-front wavefunctions and distribution amplitudes

Our starting point is the definition of the distribution amplitudes (DAs) of light pseudoscalar meson [1, 48]. The DAs parameterize the operator product expansion of meson-to-vacuum matrix elements [49],

$$\langle 0|\bar{q}(0)\gamma_\mu\gamma_5q(x)|P(p)\rangle = if_P p_\mu \int_0^1 du e^{-iup\cdot x}\Phi(u), \quad (4)$$

$$\langle 0|\bar{q}(0)i\gamma_5q(x)|P(p)\rangle = f_P \mu_P \int_0^1 du e^{-iup\cdot x}\phi(u), \quad (5)$$

where  $\mu_P = m_P^2/(\bar{m}_q + \bar{m}_{\bar{q}})$ ,  $f_P$  is the decay constant of a pseudoscalar ( $P$ ) meson, and  $\Phi(u)$  and  $\phi(u)$  are the twist-2 and twist-3 DAs, respectively.

In the following derivation, we will adopt the Lepage-Brodsky (LB) convention [1, 48] and assume the light-front gauge,  $A^+ = 0$ . At equal LF time, the DAs can be expressed using Eqs. (4) and (5) as

$$f_P \Phi(z, \mu) = -\frac{i}{2} \int dx^- e^{izp^+x^-/2} \langle 0|\bar{q}(0)\gamma^+\gamma_5q(x^-)|P(p)\rangle, \quad (6)$$

$$\mu_P f_P \phi(z, \mu) = \frac{i}{2} p^+ \int dx^- e^{izp^+x^-/2} \langle 0|\bar{q}(0)\gamma_5q(x^-)|P(p)\rangle, \quad (7)$$

by performing the Fourier transformation with respect to  $x^- = x^0 - x^3$ . The remaining main task is to cope with the hadronic matrix elements involved in Eqs. (6) and (7).

In the framework of LF quantization [1, 48], a hadronic eigenstate  $|P\rangle$  can be expanded on a complete Fock-state basis of noninteracting 2-particle states as

$$|P\rangle = \sum_{h,\bar{h}} \int \frac{dk^+ d^2\mathbf{k}_\perp}{(2\pi)^3 2\sqrt{k^+(p^+ - k^+)}} \Psi_{h,\bar{h}}^P(k^+/p^+, \mathbf{k}_\perp) |k^+, k_\perp, h; p^+ - k^+, -k_\perp, \bar{h}\rangle, \quad (8)$$

in which  $\Psi_{h,\bar{h}}^P$  is the LFWF of pseudoscalar meson with the helicity-dependence included, and  $h$  and  $\bar{h}$  denote the helicities of quark and anti-quark, respectively. The one-particle state is defined, for instance, by  $|k^+\rangle = \sqrt{2k^+}b^\dagger|0\rangle$ . The Dirac (quark) field is expanded in terms of particle creation and annihilation operators as

$$\psi_+(x) = \int \frac{dk^+}{\sqrt{2k^+}} \frac{d^2\mathbf{k}_\perp}{(2\pi)^3} \sum_h [b_h(k)u_h(k)e^{-ik\cdot x} + d_h^\dagger(k)v_h(k)e^{ik\cdot x}], \quad (9)$$

with  $u_h$  and  $v_h$  being the LF helicity spinors. The equal LF-time anti-commutation relations are given by

$$\{b_h^\dagger(k), b_{h'}(k')\} = \{d_h^\dagger(k), d_{h'}(k')\} = (2\pi)^3 \delta(k^+ - k'^+) \delta^2(\mathbf{k}_\perp - \mathbf{k}'_\perp) \delta_{hh'}. \quad (10)$$

Equipped with the above formulae, the hadronic matrix element in Eqs. (6) and (7) is then expressed as

$$\begin{aligned} \langle 0 | \bar{q}(0) \Gamma q(x^-) | P(p) \rangle &= \sqrt{N_c} \sum_{h, \bar{h}} \int \frac{dk^+ d^2 \mathbf{k}_\perp \Theta(|\mathbf{k}_\perp| < \mu)}{(2\pi)^3 2\sqrt{k^+(p^+ - k^+)}} \Psi_{h, \bar{h}}^P(k^+/p^+, \mathbf{k}_\perp) \\ &\quad \times \bar{v}_{\bar{h}}(p^+ - k^+, -\mathbf{k}_\perp) \Gamma u_h(k^+, \mathbf{k}_\perp) e^{-ik^+ x^-/2}, \end{aligned} \quad (11)$$

in which  $\Gamma = \gamma^+ \gamma_5$  and  $\gamma_5$ , and the scale  $\mu$  is introduced as an ultraviolet cut-off on transverse momenta. Using Eq. (11) and integrating over  $x^-$  and  $k^+$ , we can further obtain a general expression for the RHS of Eqs. (6) and (7),

$$\begin{aligned} \int dx^- e^{izp^+ x^-/2} \langle 0 | \bar{q}(0) \Gamma q(x^-) | P(p) \rangle &= \frac{\sqrt{N_c}}{p^+} \sum_{h, \bar{h}} \int^{|\mathbf{k}_\perp| < \mu} \frac{d^2 \mathbf{k}_\perp}{(2\pi)^3} \Psi_{h, \bar{h}}^P(z, \mathbf{k}_\perp) \\ &\quad \times \left\{ \frac{\bar{v}_{\bar{h}}((1-z)p^+, -\mathbf{k}_\perp)}{\sqrt{(1-z)}} \Gamma \frac{u_h(zp^+, \mathbf{k}_\perp)}{\sqrt{z}} \right\}. \end{aligned} \quad (12)$$

To proceed with the derivation, we will need the explicit form of the holographic LFWF,  $\Psi_{h, \bar{h}}^P$ . As mentioned in the introduction, the helicity dependence of the holographic LFWF has been assumed in previous works to decouple from the dynamics, and hence  $\Psi_{h, \bar{h}}^P(z, \mathbf{k}_\perp) = \psi(z, \mathbf{k}_\perp)$ . This assumption leads to a universal formula for different kinds of mesons; however, it is obviously disfavored by experiment. In order to restore the proper helicity dependence, the holographic LFWF in the  $\mathbf{k}_\perp$  space needs to be modified as

$$\Psi_{h, \bar{h}}(z, \mathbf{k}_\perp) = N S_{h, \bar{h}}(z, \mathbf{k}_\perp) \psi(z, \mathbf{k}_\perp), \quad (13)$$

where  $S_{h, \bar{h}}(z, \mathbf{k}_\perp)$  is the helicity-dependent wavefunction,  $N$  the normalization factor determined by the normalization condition

$$\sum_{h, \bar{h}} \int dz \frac{d^2 \mathbf{k}_\perp}{2(2\pi)^3} |\Psi_{h, \bar{h}}(z, \mathbf{k}_\perp)|^2 = 1, \quad (14)$$

and  $\psi(z, \mathbf{k}_\perp)$  the radial wavefunction obtained by performing the Fourier transformation of Eq. (3),

$$\psi(z, \mathbf{k}_\perp) = \frac{4\pi}{\sqrt{\lambda}} \frac{1}{\sqrt{z(1-z)}} e^{-\frac{\mathbf{k}_\perp^2}{2\lambda z(1-z)}} e^{-\frac{1}{2\lambda} \left( \frac{m_q^2}{z} + \frac{m_{\bar{q}}^2}{1-z} \right)}. \quad (15)$$

In the case of a vector meson, one can work in analogy with the lowest-order helicity structure of the photon LFWF in QED; the following structure of  $S_{h,\bar{h}}^V$  is thus assumed [19]

$$S_{h,\bar{h}}^{V,\lambda}(z, \mathbf{k}_\perp) = \bar{u}_h(zp^+, \mathbf{k}_\perp) \not{\epsilon}^\lambda v_{\bar{h}}((1-z)p^+, -\mathbf{k}_\perp). \quad (16)$$

This form has been successfully used to study the production of  $\rho$  and  $K^*$  mesons and the decays involving the  $B \rightarrow \rho, K^*$  transitions [27, 28].

In the case of a pseudoscalar meson, following such a strategy,  $\not{\epsilon}^\lambda$  in Eq. (16) would be replaced simply by  $\gamma_5$  [50–52]. Very recently, this spin structure has been used to evaluate the pion holographic DA in Ref. [24]. The helicity-dependent wavefunction is written explicitly as

$$S_{h,\bar{h}}^P(z, \mathbf{k}_\perp) = \bar{u}_h(zp^+, \mathbf{k}_\perp)(i\gamma_5)v_{\bar{h}}(\bar{z}p^+, -\mathbf{k}_\perp), \quad \text{Scenario 1} \quad (17)$$

where the factor “ $i$ ” is now added to be consistent with the convention used in Eqs. (4) and (5), and the abbreviation  $\bar{z} = 1 - z$  is introduced for convenience. An additional multiplying factor “ $M_P$ ” kept in Ref. [24] has now been absorbed into the normalization constant in Eq. (13). It should be noted, however, that this spin structure requires the light quark and anti-quark of the pseudoscalar meson to have parallel spin projections, and thus  $L^z = \pm 1$ . This state has  $\text{twist} = 2 + L = 3$ , and is thus not the meson eigenstate of the AdS/QCD theory. Instead of  $\gamma_5$ , the Dirac structure like  $\not{p}\gamma_5$  is also allowed. We therefore consider an alternative form of  $S_{h,\bar{h}}^P$ :

$$S_{h,\bar{h}}^P(z, \mathbf{k}_\perp) = \bar{u}_h(zp^+, \mathbf{k}_\perp)(i\frac{\tilde{m}_P}{2p^+}\gamma^+\gamma_5 + i\gamma_5)v_{\bar{h}}(\bar{z}p^+, -\mathbf{k}_\perp), \quad \text{Scenario 2} \quad (18)$$

in which, the structure  $\gamma^+\gamma_5$  implies that the light quark and anti-quark have only opposite helicities. This is the helicity assignment that couples the pion to the axial-vector current and thus the pion decay constant  $f_\pi$  in  $\pi^- \rightarrow W^{*-} \rightarrow \ell^- \bar{\nu}$ . It is thus the leading-twist LFWF, and is the solution from AdS/QCD for light quarks. Since  $\tilde{m}_P$  is the invariant mass of  $q\bar{q}$  pair in the  $P$  meson, the dimensions of the two terms in  $S_{h,\bar{h}}^P$ , Eq. (18), are also consistent.

In the following, for convenience of discussion, the two helicity-dependent wavefunctions defined by Eqs. (17) and (18) will be referred to as Scenario 1 (S1) and Scenario 2 (S2), respectively. They are related by the Gell-Mann-Oakes-Renner relation and are thus not independent [53]. Using LB convention [48], the two helicity-dependent wavefunctions  $S_{h,\bar{h}}^P$  are

given explicitly as

$$S_{h,\bar{h}}^P(z, \mathbf{k}_\perp) = \begin{cases} \frac{i}{\sqrt{z\bar{z}}} [-|\mathbf{k}_\perp| e^{\mp i\theta_k} \delta_{h\pm, \bar{h}\pm} \pm (zm_{\bar{q}} + \bar{z}m_q) \delta_{h\pm, \bar{h}\mp}] , & \text{S1} \\ \frac{i}{\sqrt{z\bar{z}}} [-|\mathbf{k}_\perp| e^{\mp i\theta_k} \delta_{h\pm, \bar{h}\pm} \pm (zm_{\bar{q}} + \bar{z}m_q + z\bar{z}\tilde{m}_P) \delta_{h\pm, \bar{h}\mp}] , & \text{S2} \end{cases} \quad (19)$$

and the spinor currents in Eq. (12) can be written as

$$\frac{\bar{v}_{\bar{h}}}{\sqrt{\bar{z}}} \gamma^+ \gamma_5 \frac{u_h}{\sqrt{z}} = \pm 2p^+ \delta_{h\pm, \bar{h}\mp} , \quad (20)$$

$$\frac{\bar{v}_{\bar{h}}}{\sqrt{\bar{z}}} \gamma_5 \frac{u_h}{\sqrt{z}} = \frac{1}{z\bar{z}} [|\mathbf{k}_\perp| e^{\pm i\theta_k} \delta_{h\pm, \bar{h}\pm} \mp (zm_{\bar{q}} + \bar{z}m_q) \delta_{h\pm, \bar{h}\mp}] , \quad (21)$$

in which  $\mathbf{k}_\perp = |\mathbf{k}_\perp| e^{\pm i\theta_k}$  is specified.

Finally, in the  $\mathbf{k}_\perp$  space, using the building blocks given above, the holographic DAs of  $P$  meson can be written as

$$\Phi(z, \mu)[\text{S1}] = \frac{\sqrt{N_c}}{\pi f_P} \int^{|\mathbf{k}| < \mu} \frac{d^2 \mathbf{k}_\perp}{(2\pi)^2} \frac{N_1}{(z\bar{z})^{1/2}} (\bar{z}m_q + zm_{\bar{q}}) \psi(z, \mathbf{k}_\perp) , \quad (22)$$

$$\phi(z, \mu)[\text{S1}] = \frac{\sqrt{N_c}}{2\pi\mu_P f_P} \int^{|\mathbf{k}| < \mu} \frac{d^2 \mathbf{k}_\perp}{(2\pi)^2} \frac{N_1}{(z\bar{z})^{3/2}} \left\{ \mathbf{k}_\perp^2 + (zm_{\bar{q}} + \bar{z}m_q)^2 \right\} \psi(z, \mathbf{k}_\perp) , \quad (23)$$

for S1<sup>1</sup>, and

$$\Phi(z, \mu)[\text{S2}] = \frac{\sqrt{N_c}}{\pi f_P} \int^{|\mathbf{k}| < \mu} \frac{d^2 \mathbf{k}_\perp}{(2\pi)^2} \frac{N_2}{(z\bar{z})^{1/2}} (\bar{z}m_q + zm_{\bar{q}} + z\bar{z}\tilde{m}_P) \psi(z, \mathbf{k}_\perp) , \quad (24)$$

$$\phi(z, \mu)[\text{S2}] = \frac{\sqrt{N_c}}{2\pi\mu_P f_P} \int^{|\mathbf{k}| < \mu} \frac{d^2 \mathbf{k}_\perp}{(2\pi)^2} \frac{N_2}{(z\bar{z})^{3/2}} \left\{ \mathbf{k}_\perp^2 + (zm_{\bar{q}} + \bar{z}m_q)(zm_{\bar{q}} + \bar{z}m_q + z\bar{z}\tilde{m}_P) \right\} \psi(z, \mathbf{k}_\perp) , \quad (25)$$

for S2, where  $N_1$  and  $N_2$  are the corresponding normalization factors determined by Eq. (14). The expression in the impact space can be obtained through Fourier transformation. These formulae exhibit the connections between holographic LFDAs and LFWFs. Using the theoretical framework given above, we will present numerical results and applications of these holographic LFDAs and LFWFs in the following sections.

---

<sup>1</sup>Very recently, in Ref. [24], the pion twist-2 holographic LFDA is also evaluated with a  $S_{h,\bar{h}}^P$  similar to S1.

## 3 Input parameters and decay constants

### 3.1 Inputs

Before presenting our numerical results, we now clarify the values of input parameters used in our evaluation. One of the most important inputs is the mass scale parameter  $\sqrt{\lambda}$ <sup>2</sup>, which could be extracted from many observables. For example, to fit the light-quark mass spectrum, the values  $\sqrt{\lambda} = 0.59 \text{ GeV}$  and  $0.54 \text{ GeV}$  are suggested in Ref. [2] for light pseudoscalar and vector mesons, respectively. A mean value,  $\sqrt{\lambda} = 0.523 \text{ GeV}$ , is obtained in Ref. [16] by fitting all of the slopes of the different Regge trajectories for mesons and baryons including all excitations. This result is also favored by the recent high accuracy computation of the perturbative QCD scale parameter  $\Lambda_{\overline{\text{MS}}}$  [10]. The fit to the Bjorken sum-rule data at low  $Q^2$  yields  $\sqrt{\lambda} = 0.496 \pm 0.007 \text{ GeV}$  [54]. In Ref. [12], the value  $\sqrt{\lambda} = 0.51 \pm 0.04 \text{ GeV}$  is used for determining the freezing value of  $\alpha_s(Q^2)$  and the interface between perturbative and non-perturbative QCD. In addition, in order to describe the HERA data on diffractive  $\rho$  and  $\phi$  electroproduction, the values  $\sqrt{\lambda} = 0.55 \text{ GeV}$  and  $0.56 \text{ GeV}$  are suggested [19, 55]. Besides  $\sqrt{\lambda}$ , the light-quark masses appearing in the holographic LFWFs are the other important inputs, which will be specified below.

In this paper, for S1, we follow entirely the inputs suggested by the recent study of the pion twist-2 holographic DA with a similar LFWF of S1 [24]. Explicitly, the following input values are used [24]:

$$\sqrt{\lambda} = 523 \text{ MeV}, \quad m_s = 450 \text{ MeV}, \quad m_{u,d} = 330 \text{ MeV}, \quad \text{S1} \quad (26)$$

where the constituent quark masses are adopted, and are also used for studying the  $\rho$  and  $K^*$  mesons [27, 28]. It should be noted that, as pointed out in Ref. [2], the light-quark masses introduced in the holographic LFWF are not the traditional constituent masses in the non-relativistic theories, but the effective quark masses from the reduction of higher Fock states as functionals of the valence states. Such effective quark masses, in principle, should be universal in a specific theoretical framework of holographic QCD.

---

<sup>2</sup>In some references, the parameter  $\kappa = \sqrt{\lambda}$  is used.

Table 1: Numerical results of the  $\pi^-$  and  $K^-$  decay constants in unit of MeV.

Exp.	S1	S2	ETM	HPQCD	FL/MILC	LQCD Ave.	
[56]			[57]	[58]	[59]	[56, 60]	
$f_\pi$	$130.28 \pm 0.26$	$132.84$	$130.10^{+3.23}_{-3.77}$	—	$130.39 \pm 0.20$	—	$130.2 \pm 1.7$
$f_K$	$156.09 \pm 0.49$	$136.04$	$156.04^{+5.09}_{-4.45}$	$154.1 \pm 2.1$	$155.37 \pm 0.34$	$155.92^{+0.43}_{-0.36}$	$155.6 \pm 0.4$
$\frac{f_K}{f_\pi}$	$1.198 \pm 0.004$	$1.024$	$1.199^{+0.032}_{-0.030}$	$1.184 \pm 0.016$	$1.1916 \pm 0.0022$	$1.1956^{+0.0028}_{-0.0021}$	$1.1928 \pm 0.0026$

For S2, on the other hand, we take

$$\sqrt{\lambda} = 590 \pm 15 \text{ MeV}, \quad m_s = 272^{+69}_{-37} \text{ MeV}, \quad m_{u,d} = 79^{+7}_{-5} \text{ MeV}, \quad \text{S2} \quad (27)$$

which are obtained by fitting to the  $\pi^-$  and  $K^-$  decay constants (see the next subsection for detail). It is noted that such input values are very similar to the results,

$$\sqrt{\lambda} = 590 \text{ MeV}, \quad m_s = 357 \text{ MeV}, \quad m_{u,d} = 46 \text{ MeV}, \quad (28)$$

obtained by fitting the masses of ground states in the framework of LF holographic QCD [2].

### 3.2 Decay constants

The values of holographic parameters can be well determined by the meson decay constants. So, firstly, we present our predictions for the decay constant of pseudoscalar meson, which is defined as

$$\langle 0 | \bar{q} \gamma^\mu \gamma_5 q | P(p) \rangle = i f_P p^\mu. \quad (29)$$

Expanding the hadronic state in the same manner as in section 2, we can finally arrive at

$$f_P = \frac{\sqrt{N_c}}{\pi} \int_0^1 dz \int \frac{d^2 \mathbf{k}_\perp}{(2\pi)^2} \frac{\bar{z} m_q + z m_{\bar{q}}}{\sqrt{z \bar{z}}} N_1 \psi(z, \mathbf{k}_\perp), \quad \text{S1} \quad (30)$$

$$f_P = \frac{\sqrt{N_c}}{\pi} \int_0^1 dz \int \frac{d^2 \mathbf{k}_\perp}{(2\pi)^2} \frac{\bar{z} m_q + z m_{\bar{q}} + \bar{z} z \tilde{m}_P}{\sqrt{z \bar{z}}} N_2 \psi(z, \mathbf{k}_\perp). \quad \text{S2} \quad (31)$$

With the inputs mentioned above, our numerical results for  $f_\pi$ ,  $f_K$  and their ratio  $f_K/f_\pi$  are summarized in Table 1, in which the theoretical errors in S2 are obtained by evaluating

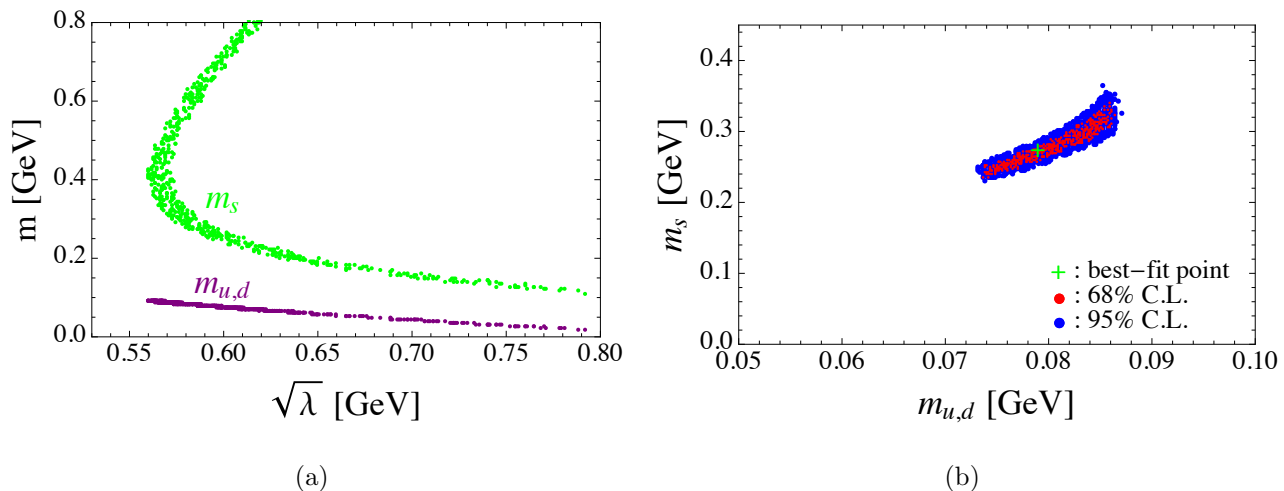


Figure 1: The fitted spaces for the holographic parameters in S2 under the constraints from the decay constants  $f_\pi$  and  $f_K$  and their ratio  $f_K/f_\pi$ . Fig. (a): the allowed spaces of  $\sqrt{\lambda}$ ,  $m_s$  and  $m_{u,d}$  at 95% C.L.; Fig. (b): the allowed spaces of  $m_s$  and  $m_{u,d}$  with  $\sqrt{\lambda} = 0.590 \pm 0.015$  GeV.

separately the uncertainties induced by each input parameter in Eq. (27) and then adding them in quadrature. For comparison, the latest experimental data [56]<sup>3</sup>, the recent results based on lattice QCD (LQCD) with  $N_f = 2+1+1$  obtained by ETM [57], HPQCD [58], Fermilab Lattice and MILC (FL/MILC) [59] Collaborations, and the world averaged results of LQCD [56, 60] are also listed in Table 1.

In S1, our result  $f_\pi = 132.84$  MeV is comparable with the data and, as found in Ref. [24], achieves a much better agreement than that obtained without helicity improvement. However, S1 results in very small results for kaon,  $f_K = 136.04$  MeV and  $f_K/f_\pi = 1.024$ , which deviate far from the data. In fact, no matter what values of the light-quark masses are used, the predicted  $f_K/f_\pi$  in S1 is always much smaller than the data and the LQCD results. This implies that S1 cannot provide sufficient flavor-asymmetry resources. It is, however, very interesting to note that this deficiency in S1 can be remarkably improved in S2. From Table 1, it can be seen that all the results in S2 are in good agreement with the data and the LQCD results.

The decay constants  $f_\pi$  and  $f_K$  are very sensitive to the holographic parameters,  $\sqrt{\lambda}$ ,  $m_s$  and  $m_{u,d}$ , and we can, therefore, perform a  $\chi^2$ -fit for these parameters using the experimental

<sup>3</sup>The values  $|V_{ud}| = 0.9758 \pm 0.0016$  and  $|V_{us}| = 0.2248 \pm 0.0006$  [56] are used to obtain the experimental data on  $f_\pi$  and  $f_K$ .

data on  $f_\pi$ ,  $f_K$  and  $f_K/f_\pi$  listed in Table 1. Our fitting results for  $\sqrt{\lambda}$ ,  $m_s$  and  $m_{u,d}$  at 95% C.L. are shown in Fig. 1 (a). Even though the parameter spaces could not be seriously constrained due to the limited constraining conditions, we do obtain some useful bounds,  $m_s \gtrsim 100$  MeV,  $m_{u,d} \lesssim 100$  MeV and  $\sqrt{\lambda} > 550$  MeV. The bound  $\sqrt{\lambda} > 550$  MeV confirms the finding in Ref. [2] that a relatively larger  $\sqrt{\lambda} \sim 590$  MeV for pseudoscalar mesons is required compared with  $\sqrt{\lambda} \sim 540$  MeV for vector mesons. Thus, in our evaluation, we take the value  $\sqrt{\lambda} = 590$  MeV and assign a conservative uncertainty  $\pm 15$  MeV.

With  $\sqrt{\lambda}$  fixed at  $\sqrt{\lambda} = 590 \pm 15$  MeV, our fitted results for  $m_s$  and  $m_{u,d}$  are shown in Fig. 1 (b), and the corresponding numerical results are given by Eq. (27); another solution with unacceptably large  $m_s \sim 700$  MeV, which is allowed in principle (see Fig. 1 (a)), is discarded. It can be seen from Fig. 1 (b) that the allowed spaces are strongly constrained. Comparing Eqs. (27) with (28), we note that the fitted results for the holographic parameters match those obtained by fitting the Regge trajectories of hadrons and the ground-state masses [2].

## 4 Holographic DAs and pion-to-photon form-factor

### 4.1 Results of holographic DAs

Using the decay constants obtained above and the formulae given in section 2, we now present in Fig. 2 our predictions for the LF holographic DAs of  $\pi$  and  $K$  mesons at  $\mu = 1$  GeV and 0.5 GeV in both S1 and S2. For comparison, the asymptotic forms,  $\Phi(z) = 6z\bar{z}$  and  $\phi(z) = 1$ , and the DAs predicted by QCD sum rule (QCDSR) approach [61] are also plotted in Fig. 2.

Using the normalization factor  $N$  determined by the normalization condition for LFWF, Eq. (14), and the decay constant given by Eqs. (30) and (31), we find that our extracted twist-2 holographic DAs,  $\Phi(z, \mu)$ , for both S1 and S2 satisfy automatically the normalization condition  $\int_0^1 dz \Phi(z, \mu) = 1$ . However, the extracted twist-3 holographic DAs satisfy the condition only approximately. One of the main reasons is that, in contrast to the case of twist-2 DAs, the normalization of twist-3 holographic DAs is affected by the scale-dependent running masses of light quarks,  $\bar{m}_{q,\bar{q}}(\mu)$ , appearing in  $\mu_P$ , which have large uncertainties and are not well determined at low scales. In our evaluation, the values  $\bar{m}_s(1\text{GeV}) = 128$  MeV and  $\bar{m}_s/\bar{m}_{u,d} = 24$  are used. It should be noted that, in the evaluation of hadronic matrix elements using the

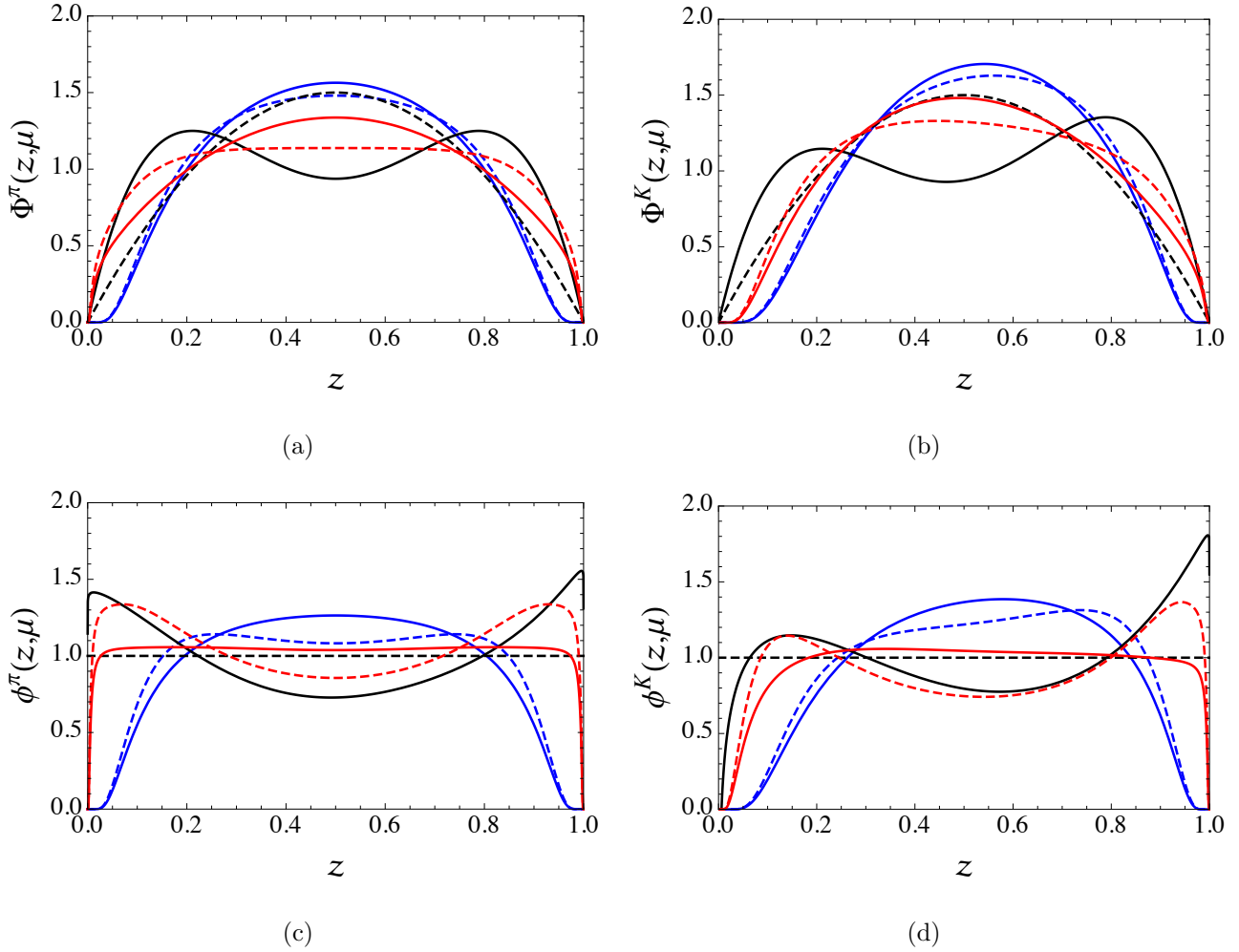


Figure 2: The holographic DAs of  $\pi$  and  $K$  mesons in S1 (blue) and S2 (red) at 0.5 GeV (dashed) and 1 GeV (solid), compared with the asymptotic forms (black dashed) and the DAs at 1 GeV in QCDSR approach (black solid).

holographic DAs, the effect of  $\bar{m}_q(\mu)$  vanishes because the factor  $\mu_P$  is cancelled, which can be clearly seen from, for instance, Eqs. (5) and (23). It also can be clearly seen from our following discussions of pure annihilation  $\bar{B}_s \rightarrow \pi^+\pi^-$  and  $\bar{B}_d \rightarrow K^+K^-$  decays.

Comparing the curves of holographic DAs at  $\mu = 0.5$  GeV and 1 GeV with each other, we can see that the effect of evolution is significant only at low scale. The evolution at large scale is, however, not obvious, as found also in the previous works [25, 26], and the perturbative evolution could be in principle recovered through the Efremov-Radyushkin-Brodsky-Lepage equation [62–64] as has been done in Ref. [65].

Table 2: The (inverse) moments of  $\pi^-$  meson at 1 GeV while for Refs. [66,67] at 2 GeV.

	S1	S2	Asym.	LFQM	QCDSR	QCDSR	LQCD	NLCQM	DES	RM
				[52]	[61]	[66]	[67]	[68]	[69]	[70]
$\langle \xi_2 \rangle$	0.172	0.238	0.2	0.24	0.286	0.343	0.269	0.21	0.28	0.28
$\langle \xi_4 \rangle$	0.062	0.116	0.086	0.11	0.143	0.181	—	0.09	0.15	0.13
$\langle z^{-1} \rangle$	2.61	3.50	3	—	3.75	4.25	—	—	5.5	—

We can also see from Fig. 2 that the twist-2 holographic DA in S2 is considerably broader than the asymptotic form, which is also expected in the other theories like QCDSR, while the one in S1 is much narrower than in S2. For the twist-3 holographic DA, its behavior in S2 at low scale is similar to the QCDSR result, while at large scale to the asymptotic form except at the regions near end-point. In contrast to the asymptotic form and the QCDSR results, the essential feature of LF holographic DAs is that they all fall rapidly to zero when  $z \rightarrow 0$  and 1, which is due to the exponential term,  $e^{-\frac{1}{2\lambda}(\frac{m_q^2}{x} + \frac{m_{\bar{q}}^2}{1-x})}$ , in the LFWF given by Eq. (15).

## 4.2 Moments and inverse moment

In order to further compare the predictions based on the holographic DAs with the ones from other non-perturbative methods, we compute the expectation values of the longitudinal momentum fraction, the  $\xi$ -moments and the inverse moment, which are defined, respectively, by

$$\langle \xi_n \rangle = \int_0^1 dz (2z - 1)^n \Phi(z, \mu), \quad \langle z^{-1} \rangle = \int_0^1 dz z^{-1} \Phi(z, \mu). \quad (32)$$

Using the central values of input parameters, our numerical results are listed in Tables 2 (for  $\pi^-$ ) and 3 (for  $K^-$ ). The theoretical predictions based on the LF quark model (LFQM) [52], the QCDSR [61, 66], the LQCD [67], the nonlocal chiral quark model (NLCQM) [68], the Dyson-Schwinger equations (DSE) [69], as well as the renormalon method (RM) [70] are also summarized in Tables 2 and 3 for comparison.

Comparing with the predictions for moments in the other theoretical models listed in Tables 2 and 3, we can see that, although the results based on the holographic DA in S1 result in

Table 3: The (inverse) moments of  $K^-$  meson at 1 GeV while for Ref. [67] at 2 GeV.

	S1	S2	Asym.	LFQM [52]	QCDSR [61]	LQCD [67]	NLCQM [68]
$\langle \xi_1 \rangle$	0.060	0.010	0	0.06	0.036	—	0.057
$\langle \xi_2 \rangle$	0.155	0.212	0.2	0.21	0.286	0.260	0.182
$\langle \xi_3 \rangle$	0.025	0.014	0	0.03	0.015	—	0.023
$\langle \xi_4 \rangle$	0.052	0.093	0.086	0.09	0.143	—	0.070
$\langle z^{-1} \rangle$	2.28	2.79	3	—	3.57	—	—

a better agreement than the ones without helicity-improvement as found in Ref. [24], they are still very small (even much smaller than the results obtained by using the asymptotic DA). As argued in Ref. [24], such discrepancies might be attributed to the fact that the dynamical spin effects are not fully captured by S1. Fortunately, as exhibited in Tables 2 and 3, we find that such discrepancies are eliminated in S2.

### 4.3 Pion-to-photon transition form factor

The pion-to-photon transition form factor can be extracted from the process  $\gamma^*(q_1)\gamma^*(q_2) \rightarrow \pi$ . In the case of only one photon being off-shell the transition form factor is denoted as  $F_{\pi\gamma}(Q^2)$  and, to the leading order in  $\alpha_s$ , is given as [48, 65]

$$F_{\pi\gamma}(Q^2) = \frac{\sqrt{2}}{3} f_\pi \int_0^1 dz \frac{\Phi^\pi(z, \bar{z}Q)}{\bar{z}Q^2}. \quad (33)$$

With both the asymptotic DA and the holographic DAs of S1 and S2, the dependence of the rescaled form factor,  $Q^2 F_{\pi\gamma}(Q^2)$ , on the photon virtuality,  $Q^2$ , are plotted in Fig. 3, in which the data from CELLO [71], CLEO [72], BaBar [73] and Belle [74] Collaborations are also shown for comparison. Even though the holographic DA of S1 does a better job than the traditional one [24], its prediction for  $Q^2 F_{\pi\gamma}(Q^2)$  is always smaller than the one obtained with asymptotic DA and is, therefore, disfavored by the BaBar [73] and Belle [74] data at large  $Q^2$  domain. Such an inconsistency could be significantly improved by the holographic DA of S2. As shown clearly in Fig. 3, the holographic DA of S2 can explain the current data in the whole

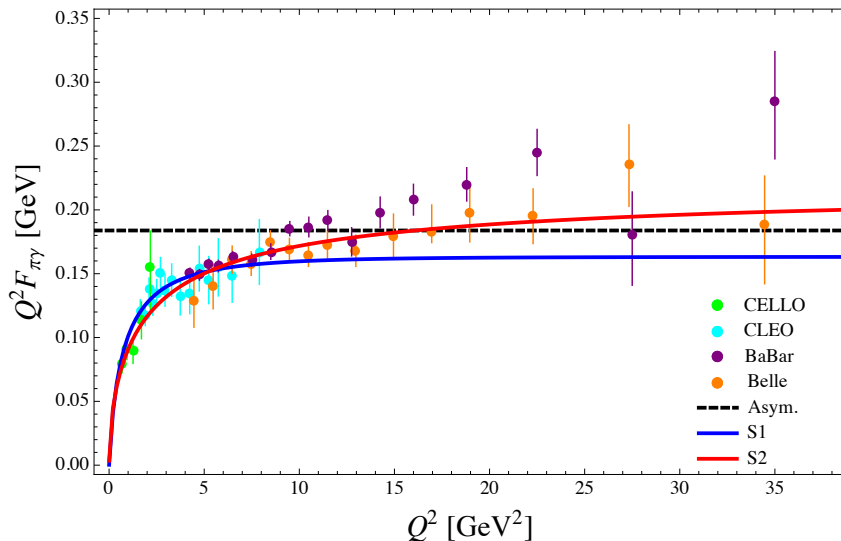


Figure 3: Theoretical predictions for  $Q^2 F_{\pi\gamma}(Q^2)$  with asymptotic DA (black dashed), holographic DAs of S1 (blue) and S2 (red), together with the comparison to the experimental data from CELLO (green) [71], CLEO (cyan) [72], BaBar (purple) [73] and Belle (orange) [74].

$Q^2$  domain, except for the BaBar result <sup>4</sup>.

## 5 Pure annihilation $\bar{B}_s \rightarrow \pi^+\pi^-$ and $\bar{B}_d \rightarrow K^+K^-$ decays

The two-body pure annihilation  $B$ -meson decays have attracted much theoretical attention during the past years, for instance, in Refs. [47, 75–86]. The experimental evidence for pure annihilation  $\bar{B}_s \rightarrow \pi^+\pi^-$  and  $\bar{B}_d \rightarrow K^+K^-$  decays was reported first by the CDF Collaboration [87], and was soon confirmed and updated by both Belle [88] and LHCb [89, 90] Collaborations. The Heavy Flavor Averaging Group (HFAG) presents the following averaged results for the branching ratios [91]:

$$\mathcal{B}(\bar{B}_s \rightarrow \pi^+\pi^-) = (6.71 \pm 0.83) \times 10^{-7}, \quad (34)$$

$$\mathcal{B}(\bar{B}_d \rightarrow K^+K^-) = (0.84 \pm 0.24) \times 10^{-7}, \quad (35)$$

---

<sup>4</sup>It should be noted that the BaBar and Belle measurements for  $Q^2 F_{\pi\gamma}(Q^2)$  at large  $Q^2$  domain are not consistent with each other.

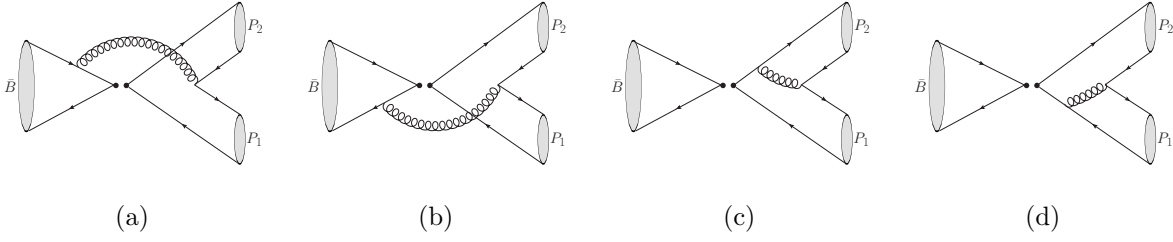


Figure 4: The leading-order Feynman diagrams for pure annihilation  $B$ -meson decays.

with the corresponding significance at the levels of about  $5\sigma$  and  $3\sigma$ , respectively. These measurements motivate accurate theoretical evaluations in different frameworks. However, due to the appearance of end-point singularities, the annihilation amplitudes are hardly to be reliably calculated. Motivated by the end-point behavior of the LF holographic DAs, we now try to evaluate the annihilation amplitudes and check if the end-point divergence can be properly controlled by LF holographic DAs.

Following the prescription proposed in Ref. [48], the hadronic matrix elements of annihilation topologies can be written as the convolution integrals of the scattering kernel with the DAs of the participating mesons [32],

$$\langle P_1 P_2 | O_i | \bar{B} \rangle = f_B f_{P_1} f_{P_2} \int dx dy d\xi \mathcal{T}_i(x, y, \xi) \varphi_{P_1}(x) \varphi_{P_2}(y) \varphi_B(\xi), \quad (36)$$

where  $O_i$  is the local four-quark operator,  $x, y$  and  $\xi$  are (anti-)quark momentum fractions, and the kernel  $\mathcal{T}_i(x, y, \xi)$  is obtained by calculating the leading-order Feynman diagrams shown in Fig. 4. In the heavy quark limit and using the collinear factorization scheme, the non-zero basic building blocks relevant to  $\bar{B}_s \rightarrow \pi^+ \pi^-$  and  $\bar{B}_d \rightarrow K^+ K^-$  decays have been fully evaluated and can be written as [44]

$$A_1 = \pi \alpha_s \int_0^1 dx dy \left\{ \Phi_{P_2}(x) \Phi_{P_1}(y) \left[ \frac{1}{y(1-x\bar{y})} + \frac{1}{\bar{x}^2 y} \right] + \frac{4}{\bar{m}_b^2(\mu)} \frac{2\tilde{\phi}_{P_2}(x)\tilde{\phi}_{P_1}(y)}{\bar{x}y} \right\}, \quad (37)$$

$$A_2 = \pi \alpha_s \int_0^1 dx dy \left\{ \Phi_{P_2}(x) \Phi_{P_1}(y) \left[ \frac{1}{\bar{x}(1-x\bar{y})} + \frac{1}{\bar{x}y^2} \right] + \frac{4}{\bar{m}_b^2(\mu)} \frac{2\tilde{\phi}_{P_2}(x)\tilde{\phi}_{P_1}(y)}{\bar{x}y} \right\}, \quad (38)$$

in which,

$$\tilde{\phi}_P(z) \equiv \mu_P \phi_P(z), \quad (39)$$

and the subscripts 1 and 2 correspond to the Dirac current structures of  $O_i$ ,  $(V-A) \otimes (V-A)$  and  $(V-A) \otimes (V+A)$ , respectively. As mentioned already, using the LF holographic DAs,

Eq. (23) in S1 or Eq. (25) in S2, one can see that the chiral factor  $\mu_P$  in Eq. (39) is cancelled out. This implies that the hadronic matrix elements,  $A_{1,2}$ , do not depend on the running masses of light-quarks when one uses the extracted LF holographic DAs.

The full amplitudes of  $\bar{B}_s \rightarrow \pi^- \pi^+$  and  $\bar{B}_d \rightarrow K^- K^+$  decays are given as

$$\mathcal{A}(\bar{B} \rightarrow P_1 P_2) = \sum_{p=u,c} B_{P_1 P_2}^p \left[ (\delta_{pu} b_1^p + b_4^p + b_{4,\text{EW}}^p)_{P_1 P_2} + \left( b_4^p - \frac{1}{2} b_{4,\text{EW}}^p \right)_{P_2 P_1} \right], \quad (40)$$

with  $P = \pi, K$ , and

$$B_{\pi\pi}^p = i \frac{G_F}{\sqrt{2}} V_{pb} V_{ps}^* f_{B_s} f_{P_1} f_{P_2}, \quad B_{KK}^p = i \frac{G_F}{\sqrt{2}} V_{pb} V_{pd}^* f_{B_d} f_{P_1} f_{P_2}, \quad (41)$$

$$b_1^p = \frac{C_F}{N_c^2} C_1 A_1, \quad b_4^p = \frac{C_F}{N_c^2} [C_4 A_1 + C_6 A_2], \quad b_{4,\text{EW}}^p = \frac{C_F}{N_c^2} [C_{10} A_1 + C_8 A_2], \quad (42)$$

in which  $V_{pb} V_{ps}^*$  and  $V_{pb} V_{pd}^*$  ( $p = u, c$ ) are the product of the Cabibbo-Kobayashi-Maskawa (CKM) matrix elements [92, 93], and  $C_i$  the scale-dependent Wilson coefficients. We use the subscripts  $P_1 P_2$  and  $P_2 P_1$  in Eq. (40) to indicate that the first meson contains the anti-quark emitted from the weak vertex and having momentum fraction  $\bar{y}$ , while another quark emitted from the weak vertex has momentum fraction  $x$ .

From Eqs. (37) and (38), one finds that the end-point divergence appears when the asymptotic DA,  $\phi(z) = 1$ , or any other forms of DA having non-vanishing end-point behavior are adopted, *i.e.*,

$$\lim_{\bar{x} \text{ or } y \rightarrow 0} \frac{\phi_{P_2}(x) \phi_{P_1}(y)}{\bar{x} y} \sim \lim_{\bar{x} \text{ or } y \rightarrow 0} \frac{1}{\bar{x} y} \rightarrow \infty. \quad (43)$$

Traditionally, these integrals are usually parameterized by a complex parameter  $X_A$ , according to  $\int_0^1 dx/x \rightarrow X_A = (1 + \rho_A e^{i\phi_A}) \ln(m_B/\Lambda_h)$  [44]. As mentioned already, in the framework of LF holographic QCD, the end-point divergence can be well controlled because it is regulated naturally by the exponential factor involving the effective quark masses in the LFWF.

In the numerical evaluations, we will use the values of CKM parameters fitted by the CKMfitter group [94],

$$A = 0.8227_{-0.0136}^{+0.0066}, \quad \lambda = 0.22543_{-0.00031}^{+0.00042}, \quad \bar{\rho} = 0.1504_{-0.0062}^{+0.0121}, \quad \bar{\eta} = 0.3540_{-0.0076}^{+0.0069}, \quad (44)$$

the averaged values of the  $B$ -meson decay constants [56],

$$f_{B_s} = 227.2 \pm 3.4 \text{ MeV}, \quad f_{B_d} = 190.9 \pm 4.1 \text{ MeV}, \quad (45)$$

Table 4: The CP-averaged branching ratios of  $\bar{B}_s \rightarrow \pi^+\pi^-$  and  $\bar{B}_d \rightarrow K^+K^-$  decays in unit of  $10^{-7}$ . For the results of S2, the first, second and third theoretical errors are caused by uncertainties of the CKM parameters and  $B$ -meson decay constants, the holographic parameters in Eq. (27), and the renormalization scale  $\mu$ , respectively.

Decay Mode	Exp. [91]	S1	S2	QCDF [44]	pQCD [76]
$\bar{B}_s \rightarrow \pi^+\pi^-$	$6.71 \pm 0.83$	0.220	$6.81_{-0.46-1.29-3.44}^{+0.54+1.33+18.41}$	$0.24_{-0.03-0.12-0.21}^{+0.03+0.25+1.63}$	$5.10_{-1.68-0.19-0.83-0.20}^{+1.96+0.25+1.05+0.29}$
$\bar{B}_d \rightarrow K^+K^-$	$0.84 \pm 0.24$	0.023	$0.23_{-0.02-0.06-0.09}^{+0.03+0.06+0.42}$	$0.13_{-0.05-0.05-0.11}^{+0.05+0.08+0.87}$	$1.56_{-0.42-0.22-0.19-0.09}^{+0.44+0.23+0.22+0.13}$

and the central values of the other inputs, such as the well-determined masses and lifetimes of  $B$  mesons, and the Fermi constant *etc.*, given by PDG [56]. Using these inputs, our numerical results for the CP-averaged branching ratios of  $\bar{B}_s \rightarrow \pi^+\pi^-$  and  $\bar{B}_d \rightarrow K^+K^-$  decays are listed in Table 4, in which the experimental data and the previous theoretical results based on the QCDF with parameterization scheme [44] and the pQCD [76] approaches are also given for comparison. Our results are evaluated at the renormalization scale  $\mu \sim \bar{m}_b/2 = 2.09 \text{ GeV}$  with an assigned uncertainty  $\pm 1 \text{ GeV}$ . The theoretical errors caused by the CKM parameters and  $B$ -meson decay constants, the holographic inputs given by Eq. (27), and the renormalization scale  $\mu$  are obtained by evaluating separately the uncertainties induced by each input parameter and then adding them in quadrature.

From Table 4, we find that the results in S1 are similar to the ones obtained by using traditional parameterization scheme with  $\rho_A = 1$  [44], but are about one order of magnitude smaller than the data, which is mainly due to the fact that the holographic DAs in S1 are relatively narrow as shown in Fig. 2, and the contributions with  $z, \bar{z} \lesssim 0.2$  are strongly suppressed. In contrast, our prediction for  $\mathcal{B}(\bar{B}_s \rightarrow \pi^+\pi^-)$  in S2 is in good agreement with the data; within the experimental and theoretical uncertainties our prediction for  $\mathcal{B}(\bar{B}_d \rightarrow K^+K^-)$  also agrees with the data. This implies that S2 is much more favored by the data on  $\mathcal{B}(\bar{B}_s \rightarrow \pi^+\pi^-)$  and  $\mathcal{B}(\bar{B}_d \rightarrow K^+K^-)$ . In the following discussions, we will focus only on the results of S2.

Comparing with the previous evaluations in QCDF by using the parameterization scheme for the end-point divergence with  $\rho_A = 1$ , we find that the theoretical predictions are remarkably improved by using the holographic DAs. Comparing our predictions with the ones in pQCD, we

find good agreement for  $\mathcal{B}(\bar{B}_s \rightarrow \pi^+\pi^-)$ ; however, our result for  $\mathcal{B}(\bar{B}_d \rightarrow K^+K^-)$  is smaller than that obtained in pQCD. The significant difference between  $\mathcal{B}(\bar{B}_s \rightarrow \pi^+\pi^-)$  and  $\mathcal{B}(\bar{B}_d \rightarrow K^+K^-)$  in our evaluation can be well understood due to the following facts:

- (i) For the  $\bar{B}_s \rightarrow \pi^+\pi^-$  decay, because  $|V_{ub}V_{us}^*| \sim |A\lambda^4(\rho - i\eta)| \ll |V_{cb}V_{cs}^*| \sim A\lambda^2$ , its decay amplitude, Eq. (40), can be simplified as

$$\mathcal{A}(\bar{B}_s \rightarrow \pi^+\pi^-) \sim B_{\pi\pi}^c 2 (b_4^c)_{\pi^-\pi^+}, \quad (46)$$

in which  $(b_4^c)_{\pi^-\pi^+} = (b_4^c)_{\pi^+\pi^-}$  because the  $u$ - and  $d$ -quark difference is not distinguished in this paper. For the  $\bar{B}_d \rightarrow K^+K^-$  decay, on the other hand, its amplitude can be simplified as

$$\mathcal{A}(\bar{B}_d \rightarrow K^+K^-) \sim B_{KK}^u (b_1^u)_{K^-K^+} + B_{KK}^c \left[ (b_4^c)_{K^-K^+} + (b_4^c)_{K^+K^-} \right]. \quad (47)$$

Comparing with Eq. (46), one can easily find that the first and second terms in Eq. (47) are relatively suppressed by additional Cabibbo factors  $\lambda \sim 0.2$  and  $\lambda^2 \sim 0.048$ , respectively. Thus, a large ratio  $R_{\pi/K} = \mathcal{B}(\bar{B}_s \rightarrow \pi^+\pi^-)/\mathcal{B}(\bar{B}_d \rightarrow K^+K^-)$  is generally expected.

- (ii) Moreover, for the  $K^{-(+)}$  meson, as shown by Fig. 2, the holographic DAs near the endpoint where the (anti-)strange quark carries small momentum fraction is suppressed due to  $m_s > m_{u,d}$ . As a result, both twist-2 and twist-3 contributions are relatively suppressed for the  $\bar{B}_d \rightarrow K^+K^-$  compared to the  $\bar{B}_s \rightarrow \pi^+\pi^-$  decay. In addition, since  $f_{B_s} > f_{B_d}$  and the phase space of  $\bar{B}_s \rightarrow \pi^+\pi^-$  decay is larger than that of  $\bar{B}_d \rightarrow K^+K^-$  decay, the ratio  $R_{\pi/K}$  is further enhanced.

It should be noted that our evaluations are performed at leading order and the theoretical uncertainties, especially the one induced by the renormalization scale, are still quite large. Moreover, the refined measurements, especially for the  $\bar{B}_d \rightarrow K^+K^-$  decay, are required for a definite conclusion.

From the phenomenological point of view, an annihilation amplitude with a large strong phase is generally welcome in order to fit experimental data and to explain some puzzles observed in  $B$ -meson decays [79–84]. As a result, a complex parameter  $X_A$  has been introduced in the traditional parameterization scheme within the framework of QCDF [44]. By using the

dynamical gluon mass  $m_g(q^2)$  in QCDF approach [47] or by introducing transverse momentum  $k_T$  in pQCD approach [35, 36, 43], a large imaginary part in the annihilation amplitudes is also obtained because the singularities exist in the integral over momentum fractions. In contrast to the above regulation schemes, the leading-order annihilation contributions are real by using the holographic DAs. This result is understandable due to the fact that, although the leading-order annihilation corrections are evaluated at the order  $\alpha_s$ , they are in fact “tree” contributions and there is no independent internal momentum; while the strong phases are generally induced by the loop integration, such as in the vertex and penguin diagrams. In the SCET approach, real annihilation contributions of the order of  $\mathcal{O}(\alpha_s(m_b)\Lambda_{\text{QCD}}/m_b)$  have also been predicted [42]. In addition, it should be noted that complex annihilation contributions are of course possible if, for instance, final-state interactions or higher-order corrections are taken into account.

## 6 Summary

Motivated by the development of the LF holographic QCD, the LFWFs for light pseudoscalar mesons and their applications are studied in this paper. In order to restore the dynamical spin effects of quarks and to improve the predictability of LFWFs for different pseudoscalar mesons, the traditional LFWFs are modified according to two assumptions for the helicity-dependent wavefunctions, corresponding to the structures  $\bar{u}_h(i\gamma_5)v_{\bar{h}}$  (named as S1) and  $\bar{u}_h(\frac{\tilde{m}_P}{2p^+}i\gamma^+\gamma_5 + i\gamma_5)v_{\bar{h}}$  (named as S2), respectively. The LF holographic DAs of pseudoscalar mesons are then extracted using the helicity-improved LFWFs. The decay constants, the  $\xi$ -moments, the pion-to-photon transition form factor, as well as the  $\bar{B}_s \rightarrow \pi^+\pi^-$  and  $\bar{B}_d \rightarrow K^+K^-$  decays are then evaluated and compared with experiment. Our main findings are summarized as follows:

- In contrast to the LFWF for S1, we find that the LFWF for S2 can provide sufficient flavor-asymmetry resources for predicting  $f_\pi$ ,  $f_K$  and their ratio  $f_K/f_\pi$ . Moreover, the results based on S2 for all of the observables considered in this paper are in a much better agreement with experiment than the ones based on S1.
- Taking the  $\pi$  and  $K$  decay constants as constraints, we perform a  $\chi^2$ -fit for the holographic parameters, the mass scale  $\sqrt{\lambda}$  and the effective quark masses  $m_{u,d}$  and  $m_s$ . Interestingly, our fitted results are remarkably consistent with the ones obtained by fitting the Regge

trajectory of light hadrons.

- A new scheme with LF holographic DAs for regulating the end-point divergence in the annihilation amplitudes of  $B \rightarrow PP$  decays is presented. In this scheme, the leading-order annihilation contributions are real. Numerically, our predictions for the branching fractions  $\mathcal{B}(\bar{B}_s \rightarrow \pi^+\pi^-)$  and  $\mathcal{B}(\bar{B}_d \rightarrow K^+K^-)$  by using the LF holographic DAs in S2 agree well with current data and result in a relatively large flavor-symmetry breaking effect. These predictions will be further tested by future refined measurements.

## Acknowledgments

We thank Junfeng Sun at HNNU and Xingbo Yuan at KIAS for helpful discussions. This work is supported by the National Natural Science Foundation of China (Grant Nos. 11475055, 11675061 and 11435003). Q. Chang is also supported by the Foundation for the Author of National Excellent Doctoral Dissertation of P. R. China (Grant No. 201317), the Program for Science and Technology Innovation Talents in Universities of Henan Province (Grant No. 14HASTIT036), the Excellent Youth Foundation of HNNU and the CSC (Grant No. 201508410213). S.J.B. is supported by the Department of Energy, contract DE-AC02-76SF00515. SLAC-PUB-16849.

## References

- [1] S. J. Brodsky, H. C. Pauli and S. S. Pinsky, Phys. Rept. **301** (1998) 299.
- [2] S. J. Brodsky, G. F. de Teramond, H. G. Dosch and J. Erlich, Phys. Rept. **584** (2015) 1.
- [3] G. F. de Teramond and S. J. Brodsky, Phys. Rev. Lett. **94** (2005) 201601.
- [4] S. J. Brodsky and G. F. de Teramond, Phys. Rev. Lett. **96** (2006) 201601.
- [5] S. J. Brodsky and G. F. de Teramond, Phys. Rev. D **77** (2008) 056007.
- [6] S. J. Brodsky and G. F. de Teramond, Phys. Rev. D **78** (2008) 025032.
- [7] G. F. de Teramond and S. J. Brodsky, Phys. Rev. Lett. **102** (2009) 081601.

- [8] G. F. de Teramond and S. J. Brodsky, AIP Conf. Proc. **1296** (2010) 128.
- [9] V. de Alfaro, S. Fubini and G. Furlan, Nuovo Cim. A **34**, 569 (1976).
- [10] A. Deur, S. J. Brodsky and G. F. de Teramond, arXiv:1608.04933 [hep-ph].
- [11] A. Deur, S. J. Brodsky and G. F. de Teramond, Prog. Part. Nucl. Phys. **90** (2016) 1.
- [12] A. Deur, S. J. Brodsky and G. F. de Teramond, Phys. Lett. B **757** (2016) 275.
- [13] G. F. de Teramond, H. G. Dosch and S. J. Brodsky, Phys. Rev. D **91** (2015) no.4, 045040.
- [14] H. G. Dosch, G. F. de Teramond and S. J. Brodsky, Phys. Rev. D **91** (2015) no.8, 085016
- [15] S. J. Brodsky, G. F. de Teramond, H. G. Dosch and C. Lorce, Phys. Lett. B **759** (2016) 171.
- [16] S. J. Brodsky, G. F. de Teramond, H. G. Dosch and C. Lorce, Int. J. Mod. Phys. A **31** (2016) no.19, 1630029.
- [17] H. G. Dosch, G. F. de Teramond and S. J. Brodsky, Phys. Rev. D **95** (2017) no.3, 034016.
- [18] S. J. Brodsky and G. F. de Teramond, Subnucl. Ser. **45** (2009) 139.
- [19] J. R. Forshaw and R. Sandapen, Phys. Rev. Lett. **109** (2012) 081601.
- [20] T. Branz, T. Gutsche, V. E. Lyubovitskij, I. Schmidt and A. Vega, Phys. Rev. D **82** (2010) 074022.
- [21] C. W. Hwang, Phys. Rev. D **86** (2012) 014005.
- [22] A. Vega, I. Schmidt, T. Branz, T. Gutsche and V. E. Lyubovitskij, Phys. Rev. D **80** (2009) 055014.
- [23] R. Swarnkar and D. Chakrabarti, Phys. Rev. D **92** (2015) no.7, 074023.
- [24] M. Ahmady, F. Chishtie and R. Sandapen, arXiv:1609.07024 [hep-ph].
- [25] M. Ahmady and R. Sandapen, Phys. Rev. D **87** (2013) no.5, 054013.
- [26] M. Ahmady and R. Sandapen, Phys. Rev. D **88** (2013) 014042.

- [27] M. Ahmady, R. Campbell, S. Lord and R. Sandapen, Phys. Rev. D **88** (2013) no.7, 074031.
- [28] M. Ahmady, R. Campbell, S. Lord and R. Sandapen, Phys. Rev. D **89** (2014) no.7, 074021.
- [29] M. R. Ahmady, S. Lord and R. Sandapen, Phys. Rev. D **90** (2014) no.7, 074010.
- [30] M. Ahmady, S. Lord and R. Sandapen, PoS DIS **2015** (2015) 160.
- [31] M. Ahmady, S. Lord and R. Sandapen, Nucl. Part. Phys. Proc. **270-272** (2016) 160.
- [32] M. Beneke, G. Buchalla, M. Neubert and C. T. Sachrajda, Phys. Rev. Lett. **83** (1999) 1914.
- [33] M. Beneke, G. Buchalla, M. Neubert and C. T. Sachrajda, Nucl. Phys. B **591** (2000) 313.
- [34] M. Beneke, G. Buchalla, M. Neubert and C. T. Sachrajda, Nucl. Phys. B **606** (2001) 245.
- [35] Y. Y. Keum, H. N. Li and A. I. Sanda, Phys. Lett. B **504** (2001) 6.
- [36] Y. Y. Keum, H. N. Li and A. I. Sanda, Phys. Rev. D **63** (2001) 054008.
- [37] C. W. Bauer, S. Fleming, D. Pirjol and I. W. Stewart, Phys. Rev. D **63** (2001) 114020.
- [38] C. W. Bauer, D. Pirjol and I. W. Stewart, Phys. Rev. D **65** (2002) 054022.
- [39] M. Beneke, A. P. Chapovsky, M. Diehl and T. Feldmann, Nucl. Phys. B **643** (2002) 431.
- [40] M. Beneke and T. Feldmann, Phys. Lett. B **553** (2003) 267.
- [41] A. V. Manohar and I. W. Stewart, Phys. Rev. D **76** (2007) 074002.
- [42] C. M. Arnesen, Z. Ligeti, I. Z. Rothstein and I. W. Stewart, Phys. Rev. D **77** (2008) 054006.
- [43] C. D. Lu, K. Ukai and M. Z. Yang, Phys. Rev. D **63** (2001) 074009.
- [44] M. Beneke and M. Neubert, Nucl. Phys. B **675** (2003) 333.
- [45] J. f. Sun, G. h. Zhu and D. s. Du, Phys. Rev. D **68** (2003) 054003.
- [46] Q. Chang, X. Q. Li and Y. D. Yang, JHEP **0809** (2008) 038.

- [47] Q. Chang, X. W. Cui, L. Han and Y. D. Yang, Phys. Rev. D **86** (2012) 054016.
- [48] G. P. Lepage and S. J. Brodsky, Phys. Rev. D **22** (1980) 2157.
- [49] V. M. Braun and I. E. Filyanov, Z. Phys. C **48** (1990) 239.
- [50] C. Q. Geng, C. C. Lih and C. Xia, Eur. Phys. J. C **76** (2016) no.6, 313.
- [51] W. Jaus, Phys. Rev. D **41** (1990) 3394.
- [52] H. M. Choi and C. R. Ji, Phys. Rev. D **75** (2007) 034019.
- [53] S. J. Brodsky, C. D. Roberts, R. Shrock and P. C. Tandy, Phys. Rev. C **85** (2012) 065202.
- [54] G. M. Prosperi, M. Raciti and C. Simolo, Prog. Part. Nucl. Phys. **58** (2007) 387.
- [55] M. Ahmady, R. Sandapen and N. Sharma, Phys. Rev. D **94** (2016) no.7, 074018.
- [56] K. A. Olive, Chin. Phys. C **40** (2016) no.10, 100001.
- [57] N. Carrasco *et al.*, Phys. Rev. D **91** (2015) no.5, 054507.
- [58] R. J. Dowdall, C. T. H. Davies, G. P. Lepage and C. McNeile, Phys. Rev. D **88** (2013) 074504.
- [59] A. Bazavov *et al.* [Fermilab Lattice and MILC Collaborations], Phys. Rev. D **90** (2014) no.7, 074509.
- [60] S. Aoki *et al.*, Eur. Phys. J. C **77** (2017) no.2, 112.
- [61] P. Ball, V. M. Braun and A. Lenz, JHEP **0605** (2006) 004.
- [62] G. P. Lepage and S. J. Brodsky, Phys. Lett. B **87** (1979) 359.
- [63] A. V. Efremov and A. V. Radyushkin, Theor. Math. Phys. **42** (1980) 97 [Teor. Mat. Fiz. **42** (1980) 147].
- [64] A. V. Efremov and A. V. Radyushkin, Phys. Lett. B **94** (1980) 245.
- [65] S. J. Brodsky, F. G. Cao and G. F. de Teramond, Phys. Rev. D **84** (2011) 033001.

- [66] V. L. Chernyak and A. R. Zhitnitsky, Phys. Rept. **112** (1984) 173.
- [67] V. M. Braun *et al.*, Phys. Rev. D **74** (2006) 074501.
- [68] S. i. Nam, H. C. Kim, A. Hosaka and M. M. Musakhanov, Phys. Rev. D **74** (2006) 014019.
- [69] L. Chang, I. C. Cloet, J. J. Cobos-Martinez, C. D. Roberts, S. M. Schmidt and P. C. Tandy, Phys. Rev. Lett. **110** (2013) no.13, 132001.
- [70] S. S. Agaev, Phys. Rev. D **72** (2005) 114010.
- [71] H. J. Behrend *et al.* [CELLO Collaboration], Z. Phys. C **49** (1991) 401.
- [72] J. Gronberg *et al.* [CLEO Collaboration], Phys. Rev. D **57** (1998) 33.
- [73] B. Aubert *et al.* [BaBar Collaboration], Phys. Rev. D **80** (2009) 052002.
- [74] S. Uehara *et al.* [Belle Collaboration], Phys. Rev. D **86** (2012) 092007.
- [75] C. M. Arnesen, I. Z. Rothstein and I. W. Stewart, Phys. Lett. B **647** (2007) 405 Erratum: [Phys. Lett. B **653** (2007) 450].
- [76] Z. J. Xiao, W. F. Wang and Y. y. Fan, Phys. Rev. D **85** (2012) 094003.
- [77] A. Ali, G. Kramer, Y. Li, C. D. Lu, Y. L. Shen, W. Wang and Y. M. Wang, Phys. Rev. D **76** (2007) 074018.
- [78] H. Y. Cheng and C. K. Chua, Phys. Rev. D **80** (2009) 114026.
- [79] Q. Chang, J. Sun, Y. Yang and X. Li, Phys. Lett. B **740** (2015) 56.
- [80] Q. Chang, J. Sun, Y. Yang and X. Li, Phys. Rev. D **90** (2014) no.5, 054019.
- [81] C. Bobeth, M. Gorbahn and S. Vickers, Eur. Phys. J. C **75** (2015) no.7, 340.
- [82] Y. Li, W. L. Wang, D. S. Du, Z. H. Li and H. X. Xu, Eur. Phys. J. C **75** (2015) no.7, 328.
- [83] G. Zhu, Phys. Lett. B **702** (2011) 408.
- [84] K. Wang and G. Zhu, Phys. Rev. D **88** (2013) 014043.

- [85] Y. Li, C. D. Lu, Z. J. Xiao and X. Q. Yu, Phys. Rev. D **70** (2004) 034009.
- [86] Y. D. Yang, F. Su, G. R. Lu and H. J. Hao, Eur. Phys. J. C **44** (2005) 243.
- [87] T. Aaltonen *et al.* [CDF Collaboration], Phys. Rev. Lett. **108** (2012) 211803.
- [88] Y.-T. Duh *et al.* [Belle Collaboration], Phys. Rev. D **87** (2013) no.3, 031103.
- [89] R. Aaij *et al.* [LHCb Collaboration], JHEP **1210** (2012) 037.
- [90] R. Aaij *et al.* [LHCb Collaboration], Phys. Rev. Lett. **118** (2017) no.8, 081801.
- [91] Y. Amhis *et al.* [Heavy Flavor Averaging Group (HFAG) Collaboration], arXiv:1412.7515 [hep-ex], and online updates at <http://www.slac.stanford.edu/xorg/hfag/>.
- [92] N. Cabibbo, Phys. Rev. Lett. **10** (1963) 531.
- [93] M. Kobayashi and T. Maskawa, Prog. Theor. Phys. **49** (1973) 652.
- [94] J. Charles *et al.* [CKMfitter Group Collaboration], Eur. Phys. J. C **41** (2005) 1, updated results and plots available at: <http://ckmfitter.in2p3.fr>.